Search for dark photons in π^0 decays at NA48 and NA62

Francesco Gonnella[1] *

[1] Laboratori Nazionali di Frascati, via E. Fermi, 40 Frascati, 00044, Italy

Abstract: The NA48/2 experiment at CERN collected, between 2003 and 2004, $1.69 \cdot 10^7$ fully reconstructed $\pi^0 \to \gamma e^+e^-$ in the kinematic range $m_{ee} > 10$ MeV/c^2, with a negligible background contamination. The sample is analysed to search for the presence of dark photons (A') via the decay chain $\pi^0 \to \gamma A'$, $A' \to e^+e^-$. No signal is observed, and exclusion limits on space of the dark photon mass $m_{A'}$ and the mixing parameter ϵ^2 are reported.

Key words: Dark Photon, NA48, NA62

1 Introduction

Kaons are a source of tagged neutral pion decays; the opportunity for precision studies on π^0 decay physics mainly proceeds via $K^\pm \to \pi^\pm\pi^0$and $K^\pm \to \mu^\pm\pi^0\nu$ processes. One of the high-intensity kaon experiments focusing on such physics is the NA48/2 experiment at CERN SPS, which collected, between 2003 and 2004, a large sample of charged kaon ($K^\pm$) decays in flight, that is about $2 \cdot 10^{11}$ $K^\pm$ [1]. Analysing a large set of π^0 mesons decaying in the fiducial volume allows for a high-sensitivity search of the dark photon (A'), a hypothetical gauge boson appearing in hidden sectors of new physics models with an extra U(1) gauge symmetry. In such models, dark photons interact with the visible sector through kinetic mixing with the Standard Model (SM) hypercharge [2]. The observed rise in measurements of the cosmic-ray positron fraction with energy and of the $(g{-}2)$ of the muon could possibly be explained by scenarios involving GeV-scale dark matter and therefore dark photons [3]. A recent review of the status of dark photon searches can be found in [4]. Experimentally, two parameters characterise the dark photon and are unknown *a priori*: the mixing parameter ϵ^2 and the dark photon mass $m_{A'}$. A' production in NA48/2 occurs through neutral pions coming from $K^\pm \to \pi^\pm\pi^0$ ($K_{2\pi}$) and $K^\pm \to \mu^\pm\pi^0\nu$ ($K_{\mu3}$). Dark photons may be produced and decay with the following:

$$\pi^0 \to \gamma A',\, A' \to e^+e^-; \tag{1}$$

three charged particles and a photon are produced in the final state. The expected branching ratio of the π^0 decay is [5]:

$$BR(\pi^0 \to \gamma A') = 2\epsilon^2 \left(1 - \frac{m_{A'}^2}{m_{\pi^0}^2}\right)^3 BR(\pi^0 \to \gamma\gamma); \tag{2}$$

as $m_{A'}$ approaches m_{π^0}, the branching fraction is kinematically suppressed. In the mass range accessible in this analysis, $2m_e \ll m_{A'} < m_{\pi^0}$, the dark photon lies below threshold for each decay into SM fermions, except for $A' \to e^+e^-$, whereas the $A' \to 3\gamma$ and $A' \to \nu\bar{\nu}$ processes, which are allowed loop-induced decays, are strongly suppressed. Therefore, assuming that dark photons only decay into SM particles, the only allowed fermions are two opposite-charged electrons, this leading to $BR(A' \to e^+e^-) \simeq 1$. The expected total decay width of the dark photon is [6]:

$$\Gamma(A' \to e^+e^-) = \frac{1}{3}\alpha\epsilon^2 m_{A'} \sqrt{1 - \frac{4m_e^2}{m_{A'}^2}} \left(1 + \frac{2m_e^2}{m_{A'}^2}\right). \tag{3}$$

Thus, for $2m_e \ll m_{A'} < m_{\pi^0}$, the dark photon mean lifetime $\tau_{A'}$ fulfils the relation:

$$c\tau_{A'} \simeq 0.8\mu m \left(\frac{10^{-6}}{\epsilon^2}\right)\left(\frac{100 \text{ MeV}}{m_{A'}}\right). \tag{4}$$

The NA48/2 analysis is performed assuming that dark photons decay at the production point (*prompt decay*), which is valid under two conditions: A' mass has to be sufficiently large ($m_{A'} > 10$ MeV/c^2), as well as the mixing parameter ($\epsilon^2 > 5 \cdot 10^{-7}$). Provided these, the dark photon signature is undistinguishable from the Dalitz decay $\pi^0 \to \gamma e^+e^-$ which, therefore, represents an irreducible background and determines the sensitivity of the measurement. The largest π^0_D sample is obtained through the reconstruction of the $K_{2\pi}$ and $K_{\mu3}$ processes. Furthermore, the $K^\pm \to \pi^\pm\pi^0\pi^0$ decay ($K_{3\pi}$) is considered a background in the $K_{\mu3}$ sample.

2 The NA48/2 experiment

A primary beam of 400 GeV/c protons was extracted from the CERN SPS; two simultaneous K^+ and K^- beams of narrow momentum band were delivered to the NA48/2 beam line, following a common beam axis de-

1) E-mail: francesco.gonnella@lnf.infn.it

* for the NA48/2 collaboration: Cambridge, CERN, Dubna, Chicago, Edinburgh, Ferrara, Firenze, Mainz, Northwestern, Perugia, Pisa, Saclay, Siegen, Torino, Wien.

rived from the primary beam; secondary beams with central momenta of (60±3) GeV/c (r.m.s.) were used. A 114 m-long cylindrical vacuum tank contained the fiducial volume, with a length of 98 m, in which the beam kaons decayed. A magnetic spectrometer, housed in a tank filled with helium and placed after the decay volume, measured the momenta of charged decay products. The spectrometer was made of four drift chambers (DCHs), with eight planes of sense wires each; the chambers were placed two upstream and two downstream of a dipole magnet, which provided a horizontal transverse momentum kick of 120 MeV/c to single charged particles. After the spectrometer, a plastic scintillator hodoscope (HOD) was positioned, in order to produce fast trigger signals and provide precise time measurements of charged particles. Further downstream, a liquid krypton electromagnetic calorimeter (LKr) was placed; the LKr was an almost-homogeneous ionisation chamber, $27X_0$ deep, with an active volume of 7 m^3 filled with liquid krypton; such a chamber was transversally segmented into 13248 projective 2×2 cm^2 cells, without longitudinal segmentation. The LKr information was used for photon energy measurements and charged particle identification. A hadronic calorimeter made of alternated iron and scintillator layers was located downstream, together with a muon detector system. A dedicated two-level trigger operated to collect three-track decays with an efficiency of about 98%. A detailed description of the NA48/2 experimental apparatus can be found in [7].

3 Event selection

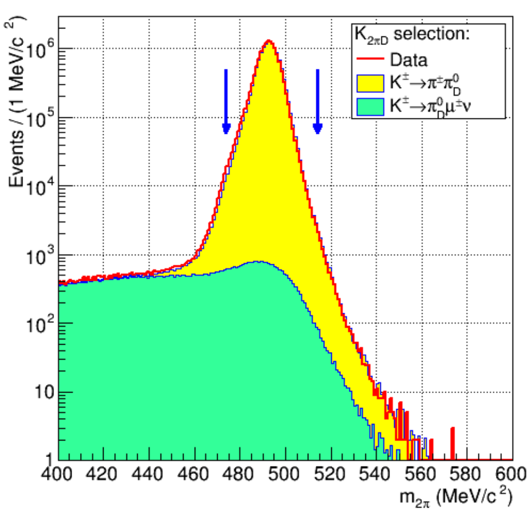

Fig. 1. Data and Monte Carlo (MC) reconstructed invariant mass of $\pi^\pm\pi^0_D$ for events passing the $K_{2\pi}$ selection. The cuts on the selection are represented by the arrows.

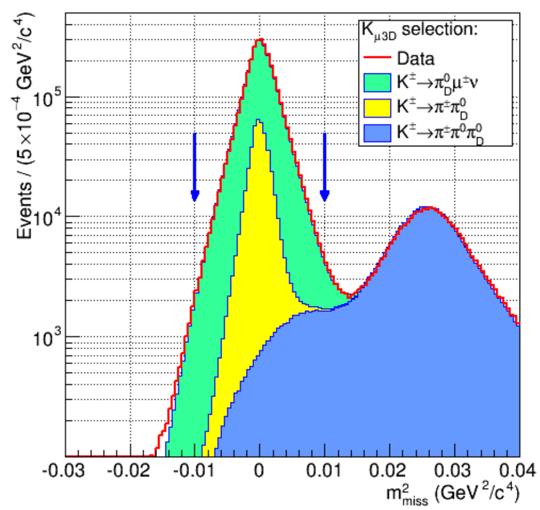

Fig. 2. Data and MC reconstructed invariant mass of $\pi^\pm\pi^0_D$ for events passing the $K_{\mu3}$ selection. The cuts on the selection are represented by the arrows.

For the analysis presented in this paper, the whole NA48/2 data sample was used. The $K_{2\pi}$ and $K_{\mu3}$ selections, with the following $\pi^0\to\gamma e^+e^-$ event, require a three-track vertex to be reconstructed in the fiducial decay region; the vertex has to be formed by the tracks originated from a pion or muon candidate and two opposite-charged electron ($e^\pm$) candidates. The identification of charged particles is based on the ratio of energy deposition in the LKr calorimeter to the momentum measured by the spectrometer, E/p. Pions and muons are kinematically constrained above 5 GeV/c momenta, while the momentum spectra of electrons originating from π^0 decays are soft, with a peak at 3 GeV/c. Thus, the requirements for the kinematics of the process are: $p>5$ GeV/c and $E/p<0.85$ ($E/p<0.4$) for the pion (muon) candidate; $p>2.75$ GeV/c and $(E/p)_{min}<E/p<1.15$ for the electron candidates, where $(E/p)_{min}=0.80$ for $p<5$ GeV/c and $(E/p)_{min}=0.85$ otherwise. Moreover, a single insulated cluster of energy deposition in the LKr is associated to the photon candidate. The reconstructed invariant mass of the $e^+e^-\gamma$ system is required to be compatible with the π^0 mass ($|m_{e^+e^-\gamma}-m_{\pi^0}|<8$MeV/c^2), such an interval corresponding to ±5 times the resolution on $m_{e^+e^-\gamma}$.
As far as the $K_{2\pi}$ selection is concerned, the invariant mass of the $\pi^\pm e^+e^-\gamma$ system (figure 1) is to be compatible with the $K^\pm$ mass, that is 474 MeV/c^2 $<m_{\pi e^+e^-\gamma}<$ 514 MeV/c^2. Regarding the $K_{\mu3}$ selection, the squared missing mass $m^2_{miss}=(P_K-P_\mu-P_{\pi^0})^2$ (figure 2) is required to be compatible with zero, i.e. $|m^2_{miss}|<0.01$ GeV^2/c^4, where P_μ and P_{π^0} are the reconstructed four-momenta of $\mu^\pm$ and π^0, and P_K is the nominal four-momentum of the kaon.
After the two selections are applied, a sample of $1.38\cdot10^7$

($0.31{\cdot}10^7$) fully reconstructed π^0_D decay candidates, coming from $K_{2\pi}$ ($K_{\mu3}$) with a negligible background, is selected. Two parameters are used to correct the observed number of candidates: the acceptance and the trigger efficiency of the apparatus; eventually, the total number of $K^\pm$ decays in the 98 m-long fiducial region for the analysed data sample is found to be $N_K = (1.57 \pm 0.05) \cdot 10^7$, where the external uncertainty on the π^0_D decay branching fraction dominates the error on N_K.

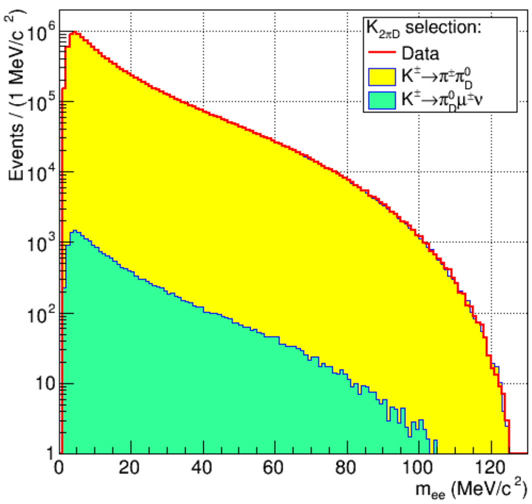

Fig. 3. Data and MC reconstructed invariant mass m_{ee} for events passing the $K_{2\pi}$ selection.

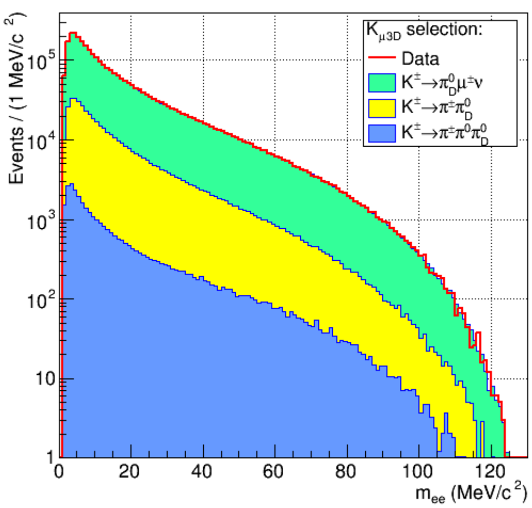

Fig. 4. Data and MC reconstructed invariant mass m_{ee} for events passing the $K_{\mu3}$ selection.

Figure 3 shows the reconstructed spectra of the e^+e^- invariant mass for the $K_{2\pi}$ selection, while figure 4 displays the same reconstructed spectra for the $K_{\mu3}$ selection; in addition to the two single selections, a joint dark photon selection is taken into account and considered passed whenever an event fulfils either the $K_{2\pi}$ or the $K_{\mu3}$ requirements. The acceptance of the joint selection for any process is equal to the sum of the acceptances of the two mutually exclusive individual selections.

4 The π^0 Dalitz simulation

The π^0_D decay is simulated using the following lowest-order differential decay rate:

$$\frac{d^2\Gamma}{dxdy} = \Gamma_0 \frac{\alpha}{\pi} |F(x)|^2 \frac{(1-x)^3}{4x} \left(1 + y^2 + \frac{r^2}{x}\right), \tag{5}$$

where x and y are two kinematic variables defined as:

$$x = \frac{(q_1 + q_2)^2}{m_\pi^2} = \frac{m_{ee}^2}{m_{\pi^0}^2},\; y = \frac{2p(q_1 - q_2)}{m_{\pi^0}(1-x)}. \tag{6}$$

In these definitions, $r = 2m_e/m_{\pi^0}$, whereas q_1, q_2 and p are the four-momenta of the opposite-charged electrons and the neutral pion; Γ_0 is the rate of the $\pi^0 \to \gamma\gamma$ decay, and $F(x)$ is the transition form factor (TFF) of the pion. According to the classical approach of Mikaelian and Smith [8], one can implement radiative corrections to the differential decay rate, which is thereby modified using the following formula:

$$\frac{d^2\Gamma^{rad}}{dxdy} = \delta(x,y)\frac{d^2\Gamma}{dxdy}, \tag{7}$$

which does not take into account the emission of inner bremsstrahlung photons.
The TFF is conventionally parametrised as $F(x) = 1 + ax$, where the slope parameter of the TFF, a, is expected to be of about 0.03, according to vector meson dominance models; detailed theoretical computations based on the dispersion theory yield $a = 0.0307 \pm 0.0006$ [9]. Experimentally, the Particle Data Group provides a measurement of $a = 0.032 \pm 0.004$ [10], mainly determined by the CELLO experiment [11], which measured the rate of the $e^+e^- \to e^+e^-\pi^0$ process in the space-like region.
However, the precision on the Mikaelian and Smith radiative corrections to the π^0_D decay is limited: indeed, the measured TFF slope lacks of a further correction, due to two-photon exchange, which is estimated to be $\Delta a = +0.005$ [12]. For this reason, the description of the backgrounds cannot benefit from precise inputs on the TFF slope [9, 10]; therefore, by fitting the data of the m_{ee} spectrum itself, an effective TFF slope is obtained and used to get a satisfactory background description, as evaluated by a χ^2 test, over the range $m_{ee} > 10\,\mathrm{MeV/c^2}$, the one used in the search for the dark photon. The acceptance computation in the m_{ee} region is less robust due to two reasons: the abruptly falling geometrical acceptance at low values of m_{ee} and the decreasing efficiency in identifying electrons at low momentum; this accounts for the fact that the m_{ee} region is not considered for the aforementioned purpose.

5 Search for the dark photon

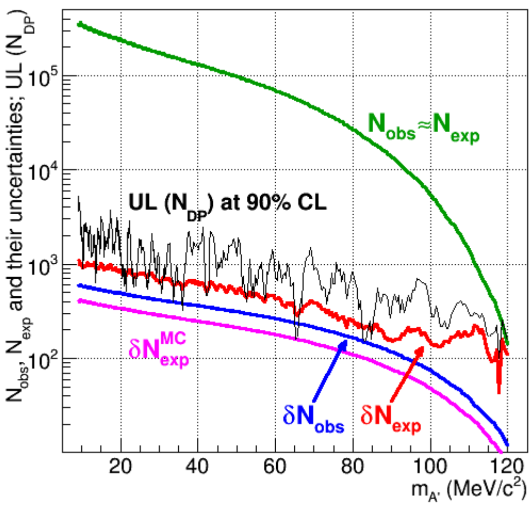

Fig. 5. Numbers of observed data events and expected π^0_D background events passing the joint selection (indistinguishable in a logarithmic scale), estimated uncertainties and obtained upper limits at 90% CL on the numbers of dark photon candidates (N_{DP}) for each mass value $m_{A'}$.

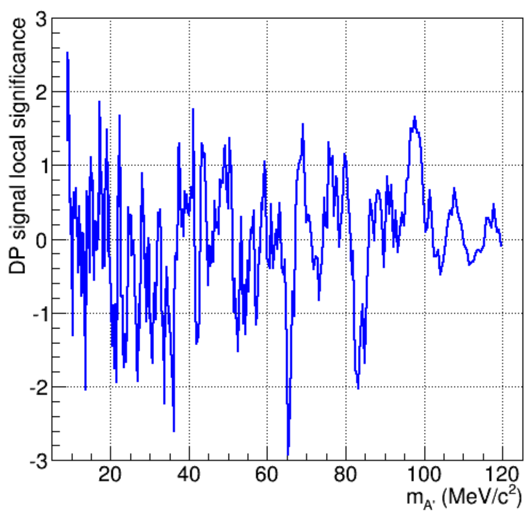

Fig. 6. Estimated local significance of the dark photon signal for each A' mass value.

In the mass range 9 MeV/c^2 $\leq m_{A'} <$ 120 MeV/c^2, a scan to search for dark photon signals is performed. The limited precision of MC simulations on backgrounds at low mass affects the lower extent of the considered mass range, whereas the signal acceptance drops to zero at the upper limit of the range. The mass step of the scan and the width of the mass window for the dark photon signal, around the assumed mass, are determined by the resolution δm_{ee} on the e^+e^- invariant mass, which is a function of m_{ee} to be evaluated with MC simulations; this function is parametrised as $\sigma_m(m_{ee}) = 0.067\,\mathrm{MeV/c^2} + 0.0105 m_{ee}$, and varies between 0.16 MeV/c^2 and 1.33 MeV/c^2 over the mass range of the scan, whose mass step is set to be $\sigma_m/2$, while the mass window of the signal region, for each hypothesis on the dark photon mass, is defined as $\pm 1.5\sigma_m$ around the assumed mass. The width of such a mass window has been optimised via MC simulations, in order to obtain the highest possible sensitivity on the dark photon signal; both the fluctuation of π^0_D background and the signal acceptance contribute to the determination of the sensitivity.

Each mass value of the dark photon is considered, studying the number of observed events passing the joint selection, N_{obs}, and comparing them to the expected number of background events, N_{exp}. The latter is evaluated from MC simulations and corrected for the trigger efficiency, as measured from control data samples passing the joint selection. Figure 5 shows the numbers of observed and expected events for each mass value and their estimated uncertainties, δN_{obs} and δN_{exp}, being the former equal to $\sqrt{N_{obs}}$, because of its statistical origin; on the other hand, the generated MC sample is rather limited, this contributing to the determination of δN_{exp}, together with the statistical errors on the trigger efficiencies, measured in the signal region of the dark photon. One can evaluate the local statistical significance of the dark photon signal for each mass value (figure 6):

$$Z = (N_{obs} - N_{exp}) / \sqrt{(\delta N_{obs})^2 + (\delta N_{exp})^2}. \quad (8)$$

The measurements of N_{obs}, N_{exp} and δN_{exp} allow for the computation of confidence intervals at 90% CL on the number of $A' \to e^+e^-$ decay candidates, called N_{DP}, for each mass hypothesis; this calculation is performed by using the Rolke-Lopez method [13], assuming Poissonian (Gaussian) errors on the number of observed (expected) events.

Furthermore, under the assumption $BR(A' \to e^+e^-) = 1$, one can also compute upper limits at 90% CL on the branching fraction $BR(\pi^0 \to A'\gamma)$, considering each mass value of the dark photon; the above-mentioned presumption is a good approximation for $m_{A'} < 2m_\mu$, in case that A' decays to SM fermions only. Said upper limits are calculated making use of the following relation:

$$BR(\pi^0 \to A'\gamma) = \frac{N_{DP}}{N_K e_1 e_2 [BR(K_{2\pi}) A_{DP}(K_{2\pi}) + BR(K_{\mu 3}) A_{DP}(K_{\mu 3}) + 2BR(K_{3\pi}) A_{DP}(K_{3\pi})]}, \quad (9)$$

where $A_{DP}(K_{2\pi})$, $A_{DP}(K_{\mu 3})$ and $A_{DP}(K_{3\pi})$ are the acceptances of the joint selection for $K_{2\pi}$, $K_{\mu 3}$ and $K_{3\pi}$ decays, respectively, followed by the $\pi^0 \to A'\gamma$, $A' \to e^+e^-$ decay chain; e_1 and e_2 are the trigger inefficiencies, which have been taken into account neglecting their variations over the m_{ee} invariant mass.

One can consider the angle between the e^+ momentum (in the e^+e^- rest-frame) and the e^+e^- momentum (in the π^0 rest-frame); studying the distribution of the angle between the two momenta, one can observe that they are identical for both the dark photon (that is $\pi^0 \to A'\gamma$, $A' \to e^+e^-$) and the π^0_D decays, up to a negligible effect of the radiative corrections, which does not have to be applied in the former case, since the acceptance was found to be affected by 1% by it. Therefore, MC samples for background description are used to evaluate the dark photon acceptances, so that no dedicated MC productions are required in this analysis.

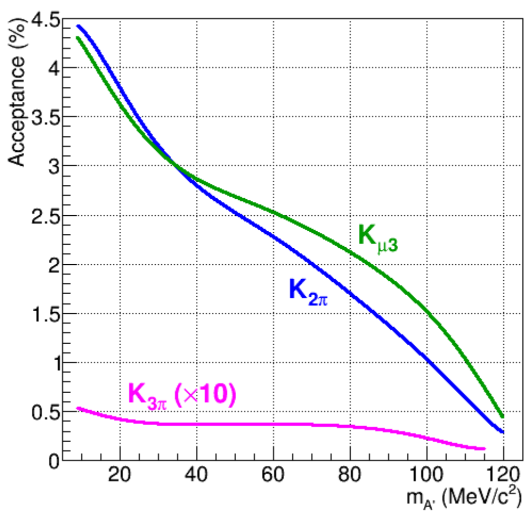

Fig. 7. Acceptances of the joint dark photon selection for $K_{2\pi}$, $K_{\mu 3}$ and $K_{3\pi}$, depending on the assumed mass of the dark photon, evaluated with MC simulations. The $K_{3\pi}$ acceptance is scaled by 10 for visibility purpose.

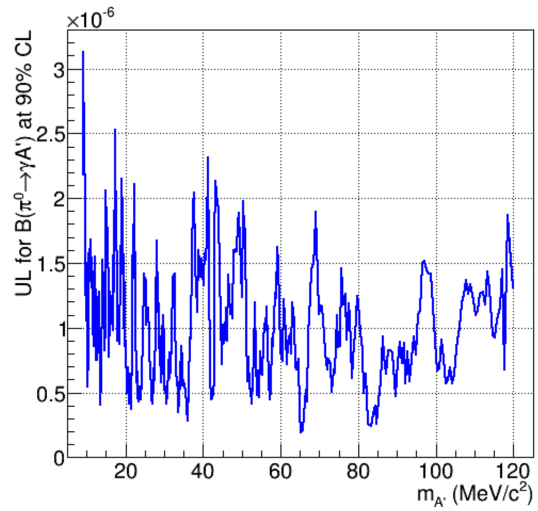

Fig. 8. Obtained upper limits on $BR(\pi^0 \to A'\gamma)$ at 90% CL, for each mass value of A'.

Figure 7 displays the resulting signal acceptances for the $\pi^0 \to A'\gamma$ decay, while figure 8 shows the upper limits on the branching ratio of the latter process, these being $O(10^{-6})$ and not exhibiting a strong dependence on $m_{A'}$.

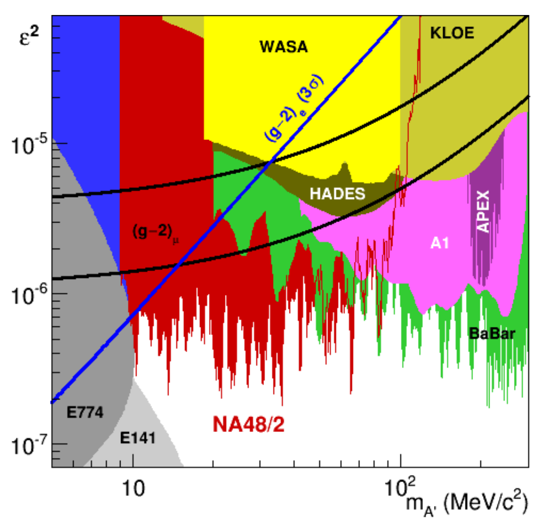

Fig. 9. The NA48/2 upper limits at 90% CL on the mixing parameter ϵ^2 versus $m_{A'}$, compared to the results on exclusion limits from meson decays, as published by SLAC E141, FNAL E774, KLOE, WASA, HADES, A1, APEX and BaBar experiments. Between black lines, the band accounting for the muon anomalous magnetic moment ($(g-2)_\mu$), whereas the blue line marks the region which could explain the anomaly of the magnetic moment of the electron ($(g-2)_e$) [14].

In figure 9, one can observe the upper limits at 90% CL on the mixing parameter ϵ^2, for each mass value of the dark photon, as computed from the upper limits on $BR(\pi^0 \to A'\gamma)$, by using equation 2; in the same figure,

one can also have a glance on the constraints obtained by SLAC E141 and FNAL E774 [15], KLOE [16], WASA [17], HADES [18], A1 [19], APEX [20] and BaBar [21] experiments. On the $(m_{A'}, \epsilon^2)$ plane, a band between the two curved lines is displayed; if the discrepancy between the measured and the calculated values for the anomalous magnetic moment of the muon lies into the $\pm 2\sigma$ range, the anomaly could be explained taking into account scenarios involving the presence of dark photons. Likewise, a region accounting for the anomalous magnetic moment of the electron is visible [3, 22].
The upper limits on ϵ^2 obtained from the present analysis represent an improvement over the existing data in the dark-photon mass range $9-70\,\mathrm{MeV/c^2}$ and exclude the whole region of $(g-2)_\mu$ [14], in the hypothesis that the dark photon can only decay into SM particles. The irreducible π^0_D background limits the sensitivity of the search for the prompt A' decay. Moreover, the achievable upper limit on ϵ^2 scales as the inverse square root of the integrated beam flux; this means that the technique with which this analysis was carried out, if applied to larger samples of K^+, as will be collected by the NA62 experiment at CERN [23] in $2015-2018$, could lead to rather modest improvements in future results.

References

1 J. R. Batley *et al.*, Eur. Phys. J. **C52**, 875 (2007).
2 B. Holdom, Phys. Lett. **B166**, 196 (1986).
3 M. Pospelov, Phys. Rev. **D80**, 095002 (2009).
4 M. Raggi and V. Kozhuharov, Riv. Nuovo Cimento, **10**, 449-505 (2015).
5 B. Batell, M. Pospelov and A. Ritz, Phys. Rev. **D80**, 095024 (2009).
6 B. Batell, M. Pospelov and A. Ritz, Phys. Rev. **D79**, 115019 (2009).
7 V. Fanti *et al.*, (NA48 collaboration), Nucl. Instrum. Meth. **A574** 433 (2007).
8 K. O. Mikaelian and J. Smith, Phys. Rev. **D5**, 1763 (1972).
9 M. Hoferichter *et al.*, Eur. Phys. J. **C74**, 3180 (2014).
10 K. A. Olive *et al.* (Particle Data Group), Chin. Phys. **C38**, 090001 (2015).
11 H. J. Behrend *et al.*, Z. Phys. **C49**, 401 (1991).
12 K. Kampf, M. Knecht and J. Novotn, Eur. Phys. J. **C46**, 191 (2006).
13 W. A. Rolke and A. M. Lopez, Nucl. Instrum. Meth. **A458**, 745 (2001).
14 J.R. Batley *et al.*, (NA48/2 collaboration), Phys. Lett. **B746**, 178-185, (2015)
15 S. Andreas, C. Niebuhr and A. Ringwald, Phys. Rev. **D86**, 095019 (2012).
16 D. Babusci *et al.*, (KLOE-2 collaboration), Phys. Lett. **B720**, 111 (2013).
17 P. Adlarson *et al.*, (WASA-at-COSY collaboration), Phys. Lett. **B726**, 187 (2013).
18 G. Agakishev *et al.*, (HADES collaboration), Phys. Lett. **B731**, 265 (2014).
19 H. Merkel *et al.*, (A1 collaboration), Phys. Rev. Lett. **112**, 221802 (2014).
20 S. Abrahamyan *et al.*, (APEX collaboration), Phys. Rev. Lett. **107**, 191804 (2011).
21 J. P. Lees *et al.*, (BaBar collaboration), Phys. Rev. Lett. **113**, 201801 (2014).
22 H. Davoudiasl, H. S. Lee and W. J. Marciano, Phys. Rev. **D89**, 095006 (2014).
23 G. Anelli et al., CERN-SPSC-2005-013.